

# Visible extreme adaptive optics on extremely large telescopes: Towards detecting oxygen in Proxima Centauri b and analogs

J. Fowler<sup>a</sup>, Sebastiaan Y. Haffert<sup>b</sup>, Maaïke A.M. van Kooten<sup>c</sup>, Rico Landman<sup>d</sup>, Alexis Bidot<sup>e</sup>, Adrien Hours<sup>e</sup>, Mamadou N'Diaye<sup>f</sup>, Olivier Absil<sup>g</sup>, Lisa Altinier<sup>h</sup>, Pierre Baudoz<sup>i</sup>, Ruslan Belikov<sup>f</sup>, Markus Johannes Bonse<sup>g, h</sup>, Kimberly Bott<sup>i, j</sup>, Bernhard Brandl<sup>d</sup>, Alexis Carlotti<sup>e</sup>, Sarah L. Casewell<sup>k</sup>, Elodie Choquet<sup>h</sup>, Nicolas B. Cowan<sup>l</sup>, Niyati Desai<sup>m</sup>, David Doelman<sup>d, n</sup>, Kevin Fogarty<sup>f</sup>, Timothy D. Gebhard<sup>g, h</sup>, Yann Gutierrez<sup>i, o, p</sup>, Olivier Guyon<sup>b, q, r, s</sup>, Olivier Herscovici-Schiller<sup>o</sup>, Roser Juanola-Parramon<sup>t, u</sup>, Matthew Kenworthy<sup>d</sup>, Elina Kleisioti<sup>d</sup>, Lorenzo König<sup>g</sup>, Mariya Krasteva<sup>v</sup>, Iva Laginja<sup>i</sup>, Lucie Leboulleux<sup>e</sup>, Johan Mazoyer<sup>g</sup>, Maxwell A. Millar-Blanchaer<sup>w</sup>, David Mouillet<sup>e</sup>, Emiel Por<sup>x</sup>, Laurent Pueyo<sup>x</sup>, Frans Snik<sup>d</sup>, Dirk van Dam<sup>d</sup>, Kyle van Gorkom<sup>b</sup>, and Sophia R. Vaughan<sup>y</sup>

<sup>a</sup>Department of Astronomy & Astrophysics, University of California, Santa Cruz, CA, USA

<sup>b</sup>Steward Observatory, University of Arizona, Tucson, AZ, USA

<sup>c</sup>National Research Council Canada, Herzberg Astronomy and Astrophysics Research Center, Victoria, Canada

<sup>d</sup>Leiden Observatory, Leiden University, Leiden, The Netherlands

<sup>e</sup>Univ. Grenoble Alpes, CNRS, IPAG, Grenoble, France

<sup>f</sup>Université Côte d'Azur, Observatoire de la Côte d'Azur, CNRS, Laboratoire Lagrange, France

<sup>g</sup>STAR Institute, Université de Liège, Liège, Belgium

<sup>h</sup>Aix Marseille Univ, CNRS, CNES, LAM, Marseille, France

<sup>i</sup>LESIA, Observatoire de Paris, Université PSL, CNRS, Sorbonne Université, Université de Paris, Meudon, France

<sup>j</sup>NASA Ames Research Center, Moffett Field, USA

<sup>k</sup>Max Planck Institute for Intelligent Systems, Tübingen, Germany

<sup>l</sup>Department of Physics, ETH Zurich, Switzerland

<sup>m</sup>University of California, Riverside

<sup>n</sup>NASA Nexus for Exoplanet System Science, Virtual Planetary Lab Team, Seattle, USA

<sup>o</sup>School of Physics and Astronomy, University of Leicester, Leicester, UK

<sup>p</sup>Department of Earth & Planetary Sciences and Department of Physics, McGill University, Montréal, QC, Canada

<sup>q</sup>Department of Astronomy, California Institute of Technology, Pasadena, CA, USA

<sup>r</sup>SRON Netherlands Institute for Space Research, Leiden, The Netherlands

<sup>s</sup>DTIS, ONERA, Université Paris Saclay, Palaiseau, France

<sup>t</sup>DOTA, ONERA, Châtillon, France

<sup>u</sup>Subaru Telescope, NAOJ, USA

<sup>v</sup>College of Optical Sciences, University of Arizona, Tucson, AZ, USA

<sup>w</sup>Astrobiology Center, Osawa, Mitaka, Tokyo, Japan

<sup>x</sup>NASA Goddard Space Flight Center, Greenbelt, MD, USA

<sup>y</sup>University of Maryland Baltimore County, 1000 Hilltop Cir, Baltimore, MD, USA

<sup>z</sup>European Space Agency, ESTEC, The Netherlands

<sup>aa</sup>Department of Physics, University of California, Santa Barbara, CA, USA

<sup>ab</sup>Space Telescope Science Institute, Baltimore, MD, USA

<sup>ac</sup>University of Oxford, UK

## ABSTRACT

Looking to the future of exo-Earth imaging from the ground, core technology developments are required in visible extreme adaptive optics (ExAO) to enable the observation of atmospheric features such as oxygen on rocky planets in visible light. UNDERGROUND (Ultra-fast AO techNOlogy Determination for Exoplanet imageRs from the GROUND), a collaboration built in Feb. 2023 at the Optimal Exoplanet Imagers Lorentz Workshop, aims to (1) motivate oxygen detection in Proxima Centauri b and analogs as an informative science case for high-contrast imaging and direct spectroscopy, (2) overview the state of the field with respect to visible exoplanet imagers, and (3) set the instrumental requirements to achieve this goal and identify what key technologies require further development.

**Keywords:** extreme adaptive optics (ExAO), extremely large telescopes (ELT), visible adaptive optics, high-contrast imaging, Earth-like planets, biosignatures, Proxima Centauri

## 1. INTRODUCTION

Finding and characterizing exo-Earths is a key science goal of Extremely Large Telescopes, specifically to explore the diversity of substellar companions, understand the formation and evolution of planetary systems, and find clues about the presence of life outside our solar system. Unlike their gas giant-planet cousins, Earth analogs will have an extremely faint self-luminous glow in the near infrared (NIR); current and future ground-based visible to NIR exoplanet imagers will not be sensitive enough to detect that thermal emission. To observe these rocky planets we must detect them in reflected light from their host star.

Proxima Centauri is a promising stellar system for reflected light studies and famous for its proximity to Earth. Proxima Centauri A is an M dwarf at 1.29 pc from our solar system that hosts the Earth-like planet Proxima Centauri b with a mass of  $1.3 M_{\oplus}$ . Our closeness to Proxima Centauri is favorable to study this system with coronagraphic observations, as planetary companions appear at larger angular separations from their host star as they get closer to Earth. For example, Proxima Centauri b has a maximum separation from its host star of 38 milli-arcseconds (mas).<sup>1</sup> Such an orbit is in theory resolvable at visible wavelengths (e.g. at  $\lambda_{O_2}=765$  nm) by current telescopes such as the VLT or Magellan ( $\lambda_{O_2}/D = 19$  mas, and  $\lambda_{O_2}/D = 24$  mas, respectively) and some initiatives exist to study these features in the Alpha Centauri system,<sup>2</sup> but the the light gathering efficiency of an 8-10 meter telescope makes high resolution spectroscopy extremely challenging. These observations become more feasible with the forthcoming extremely large observatories, with a resolution of 4 and 6 mas for the European Extremely Large Telescope (ELT) and the Giant Magellan Telescope (GMT).

While many spectral features indicate the disequilibrium chemistry that implies signs of life, oxygen is thought to be one of the strongest biosignatures, as it is the strongest marker of life in Earth's current atmosphere. The abundance of  $O_2$  closely follows the presence of life that uses oxygenic photosynthesis mechanisms. While recent research has found that there are also several abiotic processes that can generate an  $O_2$  signature, we still require the detection of  $O_2$  as a prerequisite for the presence of life.<sup>3</sup> In this work we examine the requirements to detect oxygen in the atmosphere of Proxima Centauri b using ground-based telescopes.

Section 2 describes the current state of the field for visible light adaptive optics from the ground. In Section 3.1 we outline the required contrast to detect oxygen in the atmosphere of Proxima Centauri b. In Section 3.2 we estimate a simplified AO wavefront error budget to determine the speed of the AO system before simulating the final contrast in Section 3.4. Section 4 suggests an instrument architecture and describes the remaining technology development required to reach it. Finally, in Section 5 we summarize this work and make our final conclusions.

## 2. STATE OF VISIBLE HIGH-CONTRAST IMAGING FROM THE GROUND

Only a handful of extreme Adaptive Optics (ExAO) instruments currently operate at visible wavelengths: VLT/SPHERE,<sup>4</sup> SUBARU/SCEXAO<sup>5</sup> and Magellan/MagAO-X.<sup>6,7</sup> These facilities report raw contrasts on the order of  $\sim 10^{-3}$  at 100 mas, see Table 1. The leading limitation in all systems are non common path aberrations (NCPA) which can be both static and quasi-static. To reduce the impact of these errors, one of the most crucial

developments is active focal plane wavefront control, especially the algorithms that can control mid to high-spatial frequency wavefront errors. Electric Field Conjugation (EFC) and implicit-EFC (iEFC) are examples of such dark hole digging algorithms.<sup>8-10</sup> These methods have been proven to remove quasi-static aberrations to within  $5 \times 10^{-8}$  in the lab<sup>9</sup> and  $1 \times 10^{-6}$  on sky.<sup>8</sup> After the NPCA speckles have been removed, atmospheric speckles are the ultimate limiting factor on raw contrasts.

Table 1. State of the art for visible AO performance on 8m-class telescopes.

Instrument	Contrast	Wavelength/Band	Seeing	Ref.
SPHERE/ZIMPOL	$10^{-3}$	I'	0.9"	11
SCEXAO/VAMPIRES	$5 \times 10^{-3}$	750 nm	0.55"*	12
MagAO-X	$2 \times 10^{-3}$	I	0.75"	private communication

\* As the seeing for this measurement was not recorded, we have provided the median seeing for the Mauna Kea Summit.

### 3. CONTRAST REQUIREMENTS FOR DETECTING OXYGEN

#### 3.1 Gain from high-dispersion spectroscopy

An exoplanet atmosphere is notably different from that of its host star due to a difference in atomic and molecular abundances and pressure-temperature profiles. At a high enough spectral resolution, this can be used to disentangle planet and starlight by using matched filters,<sup>13</sup> making high-dispersion spectroscopy (HDS) an efficient way to filter out starlight. However, using HDS leaves only the information content that is present in the spectral lines; there is a loss of all continuum light after filtering since the majority of the planet continuum is not different from that of its host star.

At low spectral resolution it is not possible to disentangle starlight from planet light, as stellar speckles and planets have a similar spectral shape.<sup>14</sup> In this case, a low-pass filter on the measured spectra is required to remove the influence of star light which will also remove almost all of the continuum flux of the planet.

The efficiency of HDS is defined as the ratio between the signal after and before low-pass filtering.<sup>14</sup> This efficiency for the oxygen A-band lines is shown in Figure 1, calculated with a spectral bandwidth ranging between 760 and 770 nm, corresponding to the range for the oxygen A-band. For our observing case, we assume observations of the system in the most optimistic time window, in which the influence of Earth's telluric lines are minimized.<sup>15,16</sup> The plot echoes previous results<sup>15-17</sup> that the efficiency is highest at high spectral resolution.

#### 3.2 Contrast requirements

Our science case is the detection of the oxygen A-band line in the atmosphere of Proxima Centauri b (wavelength centered at 765nm; 10nm bandwidth;  $10^{-7}$  contrast) within a single night of observation with the ELT. The instrument will need simultaneous spectra of the star and planet for removing residual star light. Since HDS post processing algorithm is a photon-noise limited method, SNR is calculated with

$$\text{SNR} = \frac{\eta T_p C F_s}{\sqrt{F_s K}} = \eta C T_p \sqrt{F_s / K}, \quad (1)$$

with efficiency of the post-processing  $\eta$ , throughput of the planet  $T_p$ , contrast between planet and star  $C$ , stellar flux  $F_s$ , and achieved raw contrast  $K$ . The main drivers for the SNR are  $\eta$ ,  $T_p$ , and  $K$ . We outline the parameters for our calculation in Table 2. This leads to a raw contrast requirement of  $3 \times 10^{-5}$ .

#### 3.3 Adaptive optics error budget

We calculate a simplified AO wavefront error budget to investigate the effects of the time delay in the AO system (i.e., the servo-lag error) on the wavefront error and Strehl ratio. From our contrast requirement in Section 3.2, we can estimate the required wavefront error (contrast is inversely proportional to the square of the wavefront error in radians for a given separation). Over the entire control radius we need to maintain a wavefront error around 45nm RMS.

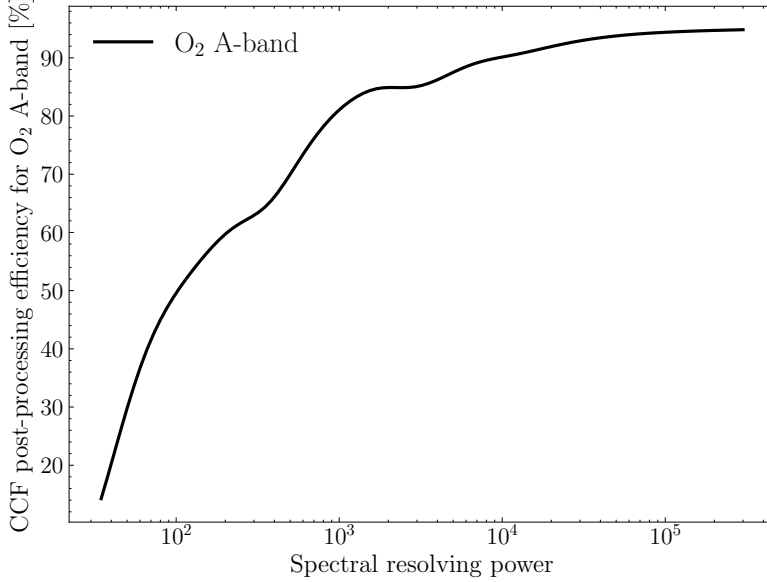


Figure 1. Efficiency of HDS post-processing as a function of resolving power. In this case we use a cross correlation function. The efficiency converges to 95% around  $R = 10^5$ .

Table 2. Parameters used to calculate the required raw contrast for Proxima Centauri b.

parameter	value used for simulations
ELT telescope area	1058.32 m
Spectrograph throughput	2 0.1 (end-to-end)
$\eta$ (HDS observing efficiency)	0.95 (from Figure 1)
Spectral bandwidth	10 nm (760 nm to 770 nm)
Contrast of Proxima Centauri b	$1 \times 10^{-7}$
Stellar magnitude of Proxima Centauri A	7.4 mag in I band
integration time	4 hours
observing goal	SNR=5

Using the analytical AO modelling software TIPTOP,<sup>18</sup> we determine the fitting error for a system using a deformable mirror (DM) with 200 actuators across the pupil diameter. Here we make the choice of using this DM actuator density to match the actuator pitch roughly to the Fried parameter  $r_0$  expected for good seeing conditions on the ELT ( $r_0 = 20$  cm). We then look at the effect of the servo-lag error on the total residual wavefront error and use that to estimate the Strehl ratio (SR) using the Marechal approximation. The largest error term is the fitting error which will be reduced for the best seeing conditions or with future technology that further increases the actuator density on wavefront correctors such as a DM. Assuming the wavefront sensor aliasing is negligible by using an optimal wavefront sensor, the next largest error term is the servo-lag error.

Table 3. RMS (root mean square) wavefront error in nm for major error terms as we vary the control speed. Assuming a 39m telescope, natural guide star (not limited by SNR/guidestar magnitude), 0.5" seeing, 10 m/s effective wind velocity, 200 actuators across the pupil diameter, and loop delay of 1 frame, at 750 nm.

Error terms at different control loop speed	1kHz	2kHz	5kHz
Fitting Error (nm RMS)	38.92	38.92	38.92
Servo-lag Error (nm RMS)	29.47	14.87	5.97
Total residual wavefront Error (nm RMS)	48.8	41.7	39.38
Strehl Ratio (Marechal approx.)	85%	89%	90%

In Table 3, we present the effects of these two terms while changing the speed of the AO system, effectively tuning the servo-lag error. We are in a regime where reducing the servo-lag error provides an important improvement in SR allowing up to 90% SR when running at 5kHz. This shows that we need to run at approximately 2kHz to achieve a wavefront error smaller than 45 nm RMS and deliver images with high Strehl ratio to the coronagraph. While minimizing the wavefront error before the coronagraph is important to achieving good contrast, we need to build on these simulations and look directly at the exact impact of the servo-lag error and our proposed system on the raw contrast; these results are shown in Section 3.4.

### 3.4 Contrast curves at varying AO loop speeds

A more detailed analysis of the performance was done by using a spatial-filter based semi-analytical approach to model the AO performance.<sup>19,20</sup> The semi-analytical approach models each aspect of the AO system as a spatial transfer function that acts onto the atmospheric Power Spectral Densities (PSDs). The final PSD is then propagated through coronagraph to get the achieved raw contrast. This is also done by using a semi-analytical approach, making this method an efficient way to generate long-exposure PSFs.<sup>21</sup> The noise on each mode is,<sup>22</sup>

$$\sigma^2 = \frac{1}{s_{pn}^2 N} + \frac{N_{sub} \sigma_{rn}^2}{s_{rn}^2 N^2}. \quad (2)$$

with  $\sigma^2$  the reconstructed wavefront variance,  $s_{pn}$  the sensitivity to photon noise,  $N_{sub}$  the number of pixels used for wavefront sensing,  $\sigma_{rn}$  the detector read noise,  $s_{rn}$  the read noise sensitivity and  $N$  the number of photons per frame.

The pyramid wavefront sensor has a sensitivity of  $\frac{1}{\sqrt{2}}$  for both photon noise and read noise.<sup>20,23</sup> We neglect the effects of amplitude errors due to scintillation and assume that there are no chromatic errors, as we plan to do wavefront sensing and science at the same wavelength. The results of the model are shown in Figure 2. Here we see that a loop speed of 2 kHz provides the best contrast at small angular separations. The aniso-server error dominates at the slower loop speed of 1 kHz and at high speeds the photon noise starts to dominate which degrades contrast. Therefore, the system should run at  $\sim 2$  kHz for optimal performance. We simulate an optimal modal gain integral controller, following some examples in the literature.<sup>20,24</sup>

### 3.5 Improvements from predictive wavefront control methods

Above we have investigated the required rate for our AO system and NCPA correction to achieve our contrast goal. However, we have not performed a photon budget analysis to determine if we will have enough signal-to-noise to run both of the loops at the desired rates. One strategy to allow the system to run slower while maintaining the high level of correction is to implement advanced control algorithms that optimize the control bandwidth without taking the measurement noise hit from shorter wavefront sensor exposures. A potential solution is predictive control. On-sky testing from Keck/NIRC2<sup>25</sup> and Subaru/SCEXAO<sup>26</sup> shows that linear predictive control methods can provide a factor of  $\sim 2-3$  in contrast as compared to an integrator when running at 1kHz. See Fowler, 2023<sup>27</sup> for an overview of predictive methods. It is also possible to run the NCPA loop with a predictive step to further improve the correction.<sup>28</sup> Perhaps more importantly however, adaptive predictive control<sup>29</sup> will allow a system to constantly adapt its controller to provide optimal control.<sup>30-32</sup> This is important as the conditions during observations are constantly changing.<sup>29</sup>

### 3.6 NCPA Correction Speed

Independent of the AO system, wavefront errors exist in the system that degrade our final performance. Specifically NCPA, whatever their origin, must be corrected to achieve good contrast. To better understand how fast we would need to run an NCPA correction, we perform a case study using an existing instrument for which the NCPA have been measured and characterized. We focus on VLT/SPHERE to determine how fast a NCPA wavefront sensor would need to run to correct for the NCPA detected by the ZELDA wavefront sensor.<sup>33</sup> From the NCPA decorrelation equations found for SPHERE for a variety of different nights, we estimate the correction frequency of the NCPA correction loop for the best and worse case scenarios. If we want to keep the NCPAs below 1 nm RMS wavefront error, to maintain a contrast of  $3 \times 10^{-5}$ , in the worse case we need to run the NCPA correction loop at 45 Hz as shown in Fig. 3.

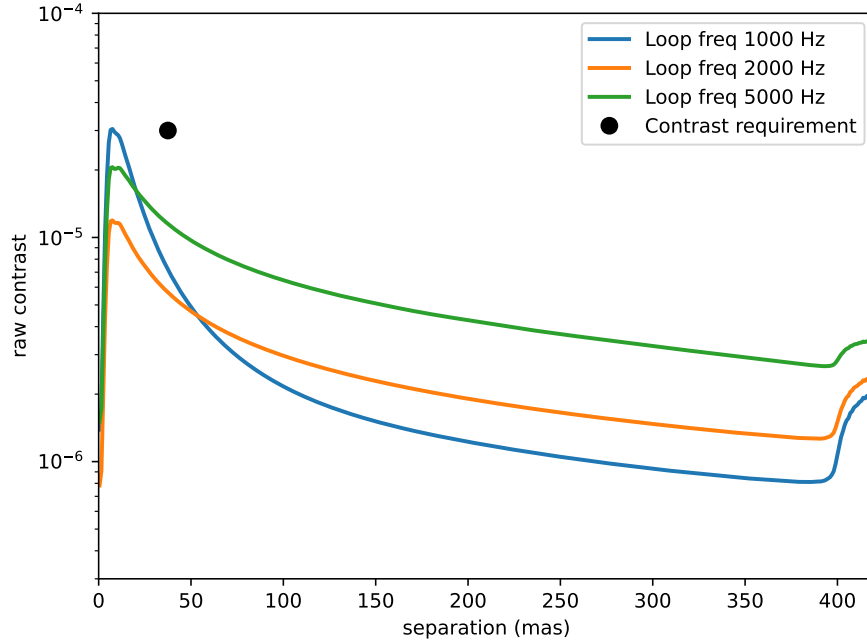


Figure 2. Raw contrast as a function of angular separation for various (1, 2, and 5 kHz) loop speeds with an unmodulated pyramid wavefront sensor (PWFS). The black dot illustrates the contrast requirement for the detection of oxygen on Proxima Centauri b. Note that 2kHz AO provides the best correction at small angular separations.

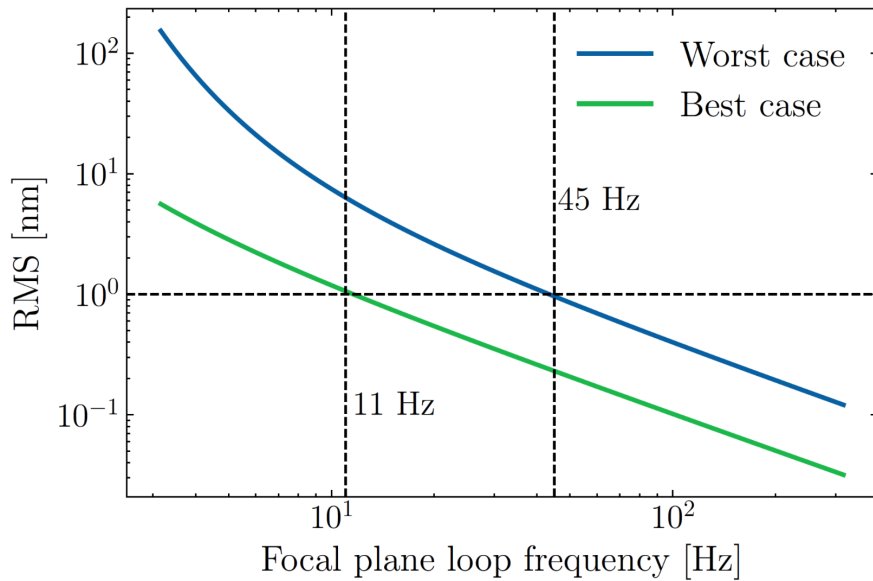


Figure 3. NCPA in RMS wavefront error as a function of the focal plane control loop frequency for different scenarios. A loop speed of 11 and 45Hz is expected to maintain a wavefront error below 1nm RMS for the NCPA and thus achieve a stable contrast of  $3 \times 10^{-5}$ .

#### 4. PROPOSED INSTRUMENT ARCHITECTURE

Here, we lay out our proposed instrument architecture for the UNDERGROUND instrument. We focus on 3 main technologies to mature: (1) optimal WFS at 2kHz, (2) fast NCPA control, and (3) high resolution spectroscopy.

Figure 4 shows the proposed instrument design for the UNDERGROUND instrument.

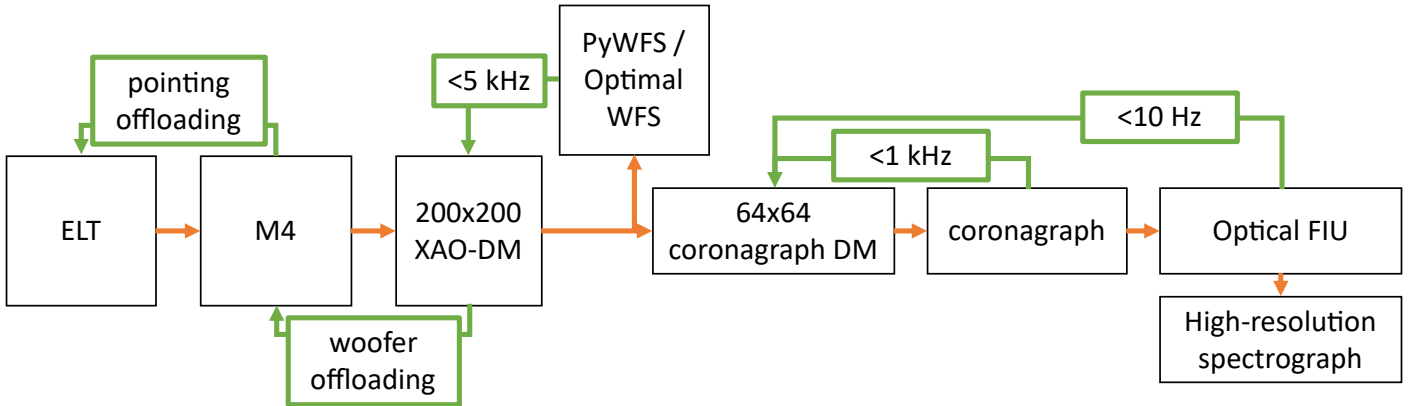


Figure 4. Schematic of the proposed UNDERGROUND instrument setup. A high-speed high-order loop corrects the atmosphere to maintain images with high Strehl ratios. A slow loop at 10 Hz creates a dark hole region where all starlight is removed. This dark hole is maintained at high speed by the wavefront sensor that is integrated into the coronagraph.

**Optimal WFS at 2kHz:** We need a high-speed high-order sensitive wavefront sensor that will control the exAO deformable mirror. This could be an un-modulated pyramid wavefront sensor,<sup>34</sup> the optimized Zernike Wavefront Sensor (ZWFS),<sup>22</sup> or the optimal PIAA-ZWFS.<sup>9</sup> Depending on the wavefront sensor, we need a different amount of pixels to sample the wavefront. The pyramid WFS requires a detector that can run at least 440x440 pixels at 2 kHz with sub-electron read-noise. Recent advances in CMOS detector technology show much promise.<sup>1</sup>

**Fast NCPA Control:** The NCPAs will be controlled by a WFS that is integrated into the coronagraph. This could be a ZWFS integrated within a Lyot-style coronagraph as demonstrated in.<sup>9,35,36</sup> The integrated control inside the coronagraph is necessary to meet the raw contrast requirements. Additionally, we added a dedicated coronagraphic DM inside the instrument to control the focal plane speckles. This will make it easier to implement EFC or iEFC because there is no need anymore to reference offset the high-order wavefront sensor. This separates the control loops of both processes making it easier to control both.

**High Resolution Spectroscopy:** There are several attractive solutions for high-resolution multi-object spectrographs, especially if only a narrow wavelength range is required. A promising option is the VIPA-style spectrograph<sup>37,38</sup> that can achieve high throughput and resolution in a compact design.

## 5. CONCLUSION

Proxima Centauri b provides an exciting opportunity to detect and characterize an Earth-like planet in visible light. With high-resolution spectroscopy, observations with future Extremely Large Telescopes could detect features like oxygen, a promising biomarker that points to life on extra-solar planets. With a contrast goal of  $3 \times 10^{-5}$  at  $10 \lambda/D$ , ground-based extreme adaptive optics combined with high-resolution multi-object spectroscopy will likely achieve this. We find that the AO system needs to exploit optimal wavefront sensing and control at  $\sim 2$ kHz and NCPA control needs to be done at tens of Hertz. To achieve all of this we outline the UNDERGROUND instrument architecture, in Section 4, that could enable the detection of oxygen for an Earth-like planet such as Proxima Centauri b.

## ACKNOWLEDGMENTS

The 2023 Optimal Exoplanet Imagers workshop, which sparked the work presented in this manuscript, was made possible thanks to the logistical and financial support of the Lorentz Center, Leiden, The Netherlands.

<sup>1</sup>The Kinetix from Teledyne can run at 3.6 kHz in high-speed mode with 440 pixel lines albeit with 2 electrons of read noise.

The research presented in this paper was initiated at a workshop held in Leiden and partially supported by NOVA (the Netherlands Research School for Astronomy) and by the European Research Council (ERC) under the European Union’s Horizon 2020 research and innovation programme (grant agreement 866001 - EXACT). SRV acknowledges funding from the European Research Council (ERC) under the European Union’s Horizon 2020 research and innovation program under grant agreement № 805445. SLC acknowledges support from an STFC Ernest Rutherford Fellowship. TDG acknowledges funding from the Max Planck ETH Center for Learning Systems. KB acknowledges support from NASA Habitable Worlds grant 80NSSC20K152, and previous support for related work from NASA Astrobiology Institute’s Virtual Planetary Laboratory under Cooperative Agreement NNA13AA93A. IL acknowledges the support by a postdoctoral grant issued by the Centre National d’Études Spatiales (CNES) in France. PB, IL, and YG were supported by the Action Spécifique Haute Résolution Angulaire (ASHRA) of CNRS/INSU co-funded by CNES. EHP is supported by the NASA Hubble Fellowship grant #HST-HF2-51467.001-A awarded by the Space Telescope Science Institute, which is operated by the Association of Universities for Research in Astronomy, Incorporated, under NASA contract NAS5-26555. LA and EC acknowledge funding from the European Research Council (ERC) under the European Union’s Horizon Europe research and innovation programme (ESCAPE, grant agreement 101044152). OA and LK acknowledge funding from the European Research Council (ERC) under the European Union’s Horizon 2020 research and innovation programme (grant agreement № 819155). SYH was funded by the generous support of the Heising-Simons Foundation. RJP is supported by NASA under award number 80GSFC21M0002. OHS acknowledges funding from the Direction Scientifique Générale de l’ONERA (ARE Alioth). This research has made use of NASA’s Astrophysics Data System Bibliographic Services and the SIMBAD database, operated at CDS, Strasbourg, France

## REFERENCES

- [1] Anglada-Escudé, G., Amado, P. J., Barnes, J., Berdiñas, Z. M., Butler, R. P., Coleman, G. A. L., de La Cueva, I., Dreizler, S., Endl, M., Giesers, B., Jeffers, S. V., Jenkins, J. S., Jones, H. R. A., Kiraga, M., Kürster, M., López-González, M. J., Marvin, C. J., Morales, N., Morin, J., Nelson, R. P., Ortiz, J. L., Ofir, A., Paardekooper, S.-J., Reiners, A., Rodríguez, E., Rodríguez-López, C., Sarmiento, L. F., Strachan, J. P., Tsapras, Y., Tuomi, M., and Zechmeister, M., “A terrestrial planet candidate in a temperate orbit around Proxima Centauri,” *Nature* **536**, 437–440 (Aug. 2016).
- [2] Kasper, M., Arsenault, R., Käufel, H. U., Jakob, G., Fuenteseca, E., Riquelme, M., Siebenmorgen, R., Sterzik, M., Zins, G., Ageorges, N., Gutruf, S., Reutlinger, A., Kampf, D., Absil, O., Carlomagno, B., Guyon, O., Klupar, P., Mawet, D., Ruane, G., Karlsson, M., Pantin, E., and Dohlen, K., “NEAR: Low-mass Planets in  $\alpha$  Cen with VISIR,” *The Messenger* **169**, 16–20 (Sept. 2017).
- [3] Meadows, V. S., Reinhard, C. T., Arney, G. N., Parenteau, M. N., Schwieterman, E. W., Domagal-Goldman, S. D., Lincowski, A. P., Stapelfeldt, K. R., Rauer, H., DasSarma, S., et al., “Exoplanet biosignatures: understanding oxygen as a biosignature in the context of its environment,” *Astrobiology* **18**(6), 630–662 (2018).
- [4] Beuzit, J. L., Vigan, A., Mouillet, D., Dohlen, K., Gratton, R., Boccaletti, A., Sauvage, J. F., Schmid, H. M., Langlois, M., Petit, C., Baruffolo, A., Feldt, M., Milli, J., Wahhaj, Z., Abe, L., Anselmi, U., Antichi, J., Barette, R., Baudrand, J., Baudoz, P., Bazzon, A., Bernardi, P., Blanchard, P., Brast, R., Bruno, P., Buey, T., Carbillet, M., Carle, M., Cascone, E., Chapron, F., Charton, J., Chauvin, G., Claudi, R., Costille, A., De Caprio, V., de Boer, J., Delboulbé, A., Desidera, S., Dominik, C., Downing, M., Dupuis, O., Fabron, C., Fantinel, D., Farisato, G., Feautrier, P., Fedrigo, E., Fusco, T., Gigan, P., Ginski, C., Girard, J., Giro, E., Gisler, D., Gluck, L., Gry, C., Henning, T., Hubin, N., Hugot, E., Incorvaia, S., Jaquet, M., Kasper, M., Lagadec, E., Lagrange, A. M., Le Coroller, H., Le Mignant, D., Le Ruyet, B., Lessio, G., Lizon, J. L., Llored, M., Lundin, L., Madec, F., Magnard, Y., Marteaud, M., Martinez, P., Maurel, D., Ménard, F., Mesa, D., Möller-Nilsson, O., Moulin, T., Moutou, C., Origné, A., Parisot, J., Pavlov, A., Perret, D., Pragt, J., Puget, P., Rabou, P., Ramos, J., Reess, J. M., Rigal, F., Rochat, S., Roelfsema, R., Rousset, G., Roux, A., Saisse, M., Salasnich, B., Santambrogio, E., Scuderi, S., Segransan, D., Sevin, A., Siebenmorgen, R., Soenke, C., Stadler, E., Suarez, M., Tiphène, D., Turatto, M., Udry, S., Vakili, F., Waters, L. B. F. M., Weber, L., Wildi, F., Zins, G., and Zurlo, A., “SPHERE: the exoplanet imager for the Very Large Telescope,” *Astron. & Astrophys.* **631**, A155 (Nov. 2019).

- [5] Jovanovic, N., Martinache, F., Guyon, O., Clergeon, C., Singh, G., Kudo, T., Garrel, V., Newman, K., Doughty, D., Lozi, J., et al., “The subaru coronagraphic extreme adaptive optics system: enabling high-contrast imaging on solar-system scales,” *Publications of the Astronomical Society of the Pacific* **127**(955), 890 (2015).
- [6] Males, J. R., Close, L. M., Miller, K., Schatz, L., Doelman, D., Lumbres, J., Snik, F., Rodack, A., Knight, J., Van Gorkom, K., et al., “Magao-x: project status and first laboratory results,” in [*Adaptive Optics Systems VI*], **10703**, 76–89, SPIE (2018).
- [7] Close, L. M., Males, J. R., Durney, O., Sauve, C., Kautz, M., Hedglen, A., Schatz, L., Lumbres, J., Miller, K., Van Gorkom, K., et al., “Optical and mechanical design of the extreme ao coronagraphic instrument magao-x,” in [*Adaptive Optics Systems VI*], **10703**, 1227–1236, SPIE (2018).
- [8] Potier, A., Mazoyer, J., Wahhaj, Z., Baudoz, P., Chauvin, G., Galicher, R., and Ruane, G., “Increasing the raw contrast of VLT/SPHERE with the dark hole technique. II. On-sky wavefront correction and coherent differential imaging,” *Astron. & Astrophys.* **665**, A136 (Sept. 2022).
- [9] Haffert, S. Y., Males, J. R., Ahn, K., Van Gorkom, K., Guyon, O., Close, L. M., Long, J. D., Hedglen, A. D., Schatz, L., Kautz, M., Lumbres, J., Rodack, A., Knight, J. M., and Miller, K., “Implicit electric field conjugation: Data-driven focal plane control,” *Astron. & Astrophys.* **673**, A28 (May 2023).
- [10] Ahn, K., Guyon, O., Lozi, J., Vievard, S., Deo, V., Skaf, N., Bragg, J. C., Haffert, S. Y., Males, J. R., and Currie, T., “Combining EFC with spatial LDFC for high-contrast imaging on Subaru/SCEAO,” *Astron. & Astrophys.* **673**, A29 (May 2023).
- [11] Schmid, H. M., Bazzon, A., Roelfsema, R., Mouillet, D., Milli, J., Menard, F., Gisler, D., Hunziker, S., Pragt, J., Dominik, C., et al., “Sphere/zimpol high resolution polarimetric imager-i. system overview, psf parameters, coronagraphy, and polarimetry,” *Astronomy & Astrophysics* **619**, A9 (2018).
- [12] Lucas, M., Bottom, M., Guyon, O., Lozi, J., Norris, B., Deo, V., Vievard, S., Ahn, K., Skaf, N., and Tuthill, P., “A visible-light Lyot coronagraph for SCEAO/VAMPIRES,” in [*Ground-based and Airborne Instrumentation for Astronomy IX*], Evans, C. J., Bryant, J. J., and Motohara, K., eds., *Society of Photo-Optical Instrumentation Engineers (SPIE) Conference Series* **12184**, 121844E (Aug. 2022).
- [13] Snellen, I., de Kok, R., Birkby, J., Brandl, B., Brogi, M., Keller, C., Kenworthy, M., Schwarz, H., and Stuik, R., “Combining high-dispersion spectroscopy with high contrast imaging: Probing rocky planets around our nearest neighbors,” *Astronomy & Astrophysics* **576**, A59 (2015).
- [14] Landman, R., Snellen, I., Keller, C., N’Diaye, M., Fagginger-Auer, F., and Desgrange, C., “Trade-offs in high-contrast integral field spectroscopy for exoplanet detection and characterisation: Young gas giants in emission,” *arXiv preprint arXiv:2305.19355* (2023).
- [15] Rodler, F. and López-Morales, M., “Feasibility studies for the detection of o<sub>2</sub> in an earth-like exoplanet,” *The Astrophysical Journal* **781**(1), 54 (2014).
- [16] Serindag, D. B. and Snellen, I. A., “Testing the detectability of extraterrestrial o<sub>2</sub> with the extremely large telescopes using real data with real noise,” *The Astrophysical Journal Letters* **871**(1), L7 (2019).
- [17] Hardegree-Ullman, K. K., Apai, D., Bergsten, G. J., Pascucci, I., and López-Morales, M., “Bioverse: A comprehensive assessment of the capabilities of extremely large telescopes to probe earth-like o<sub>2</sub> levels in nearby transiting habitable-zone exoplanets,” *The Astronomical Journal* **165**(6), 267 (2023).
- [18] Neichel, B., Beltramo-Martin, O., Plantet, C., Rossi, F., Agapito, G., Fusco, T., Carolo, E., Carla, G., Cerasuolo, M., and van der Burg, R., “Tiptop: a new tool to efficiently predict your favorite ao psf,” (2021).
- [19] Jolissaint, L., “Synthetic modeling of astronomical closed loop adaptive optics,” *arXiv preprint arXiv:1009.1581* (2010).
- [20] Males, J. R. and Guyon, O., “Ground-based adaptive optics coronagraphic performance under closed-loop predictive control,” *Journal of Astronomical Telescopes, Instruments, and Systems* **4**(1), 019001–019001 (2018).
- [21] Herscovici-Schiller, O., Mugnier, L. M., and Sauvage, J.-F., “An analytic expression for coronagraphic imaging through turbulence. application to on-sky coronagraphic phase diversity,” *Monthly Notices of the Royal Astronomical Society: Letters* **467**(1), L105–L109 (2017).
- [22] Chambouleyron, V., Fauvarque, O., Sauvage, J. F., Dohlen, K., Levraud, N., Vigan, A., N’Diaye, M., Neichel, B., and Fusco, T., “Variation on a Zernike wavefront sensor theme: Optimal use of photons,” *Astron. & Astrophys.* **650**, L8 (June 2021).

- [23] Guyon, O., “Limits of adaptive optics for high-contrast imaging,” *The Astrophysical Journal* **629**(1), 592 (2005).
- [24] Gendron, E. and Léna, P., “Astronomical adaptive optics. ii. experimental results of an optimized modal control,” *Astronomy and Astrophysics Supplement*, v. 111, p. 153 **111**, 153 (1995).
- [25] van Kooten, M. A., Jensen-Clem, R., Cetre, S., Ragland, S., Bond, C. Z., Fowler, J., and Wizinowich, P., “Predictive wavefront control on keck ii adaptive optics bench: on-sky coronagraphic results,” *Journal of Astronomical Telescopes, Instruments, and Systems* **8**(2), 029006–029006 (2022).
- [26] Currie, T., Guyon, O., Lozi, J., Groff, T., Kasdin, N. J., Martinache, F., Brandt, T. D., Chilcote, J., Marois, C., Gerard, B., Jovanovic, N., and Vievard, S., “Performance and early science with the Subaru Coronagraphic Extreme Adaptive Optics project,” in [*Society of Photo-Optical Instrumentation Engineers (SPIE) Conference Series*], *Society of Photo-Optical Instrumentation Engineers (SPIE) Conference Series* **11117**, 111170X (Sept. 2019).
- [27] Fowler, J. and Landman, R., “Tempestas ex machina: A review of machine learning methods for wavefront control,” *Society of Photo-Optical Instrumentation Engineers (SPIE) Conference Series* **in same proceedings** (2023).
- [28] Gerard, B. L., Perez-Soto, J., Chambouleyron, V., van Kooten, M. A. M., Dillon, D., Cetre, S., Jensen-Clem, R., Fu, Q., Amata, H., and Heidrich, W., “Various wavefront sensing and control developments on the Santa Cruz Extreme AO Laboratory (SEAL) testbed,” in [*Adaptive Optics Systems VIII*], Schreiber, L., Schmidt, D., and Vernet, E., eds., **12185**, 121852H, International Society for Optics and Photonics, SPIE (2022).
- [29] van Kooten, M., Doelman, N., and Kenworthy, M., “Impact of time-variant turbulence behavior on prediction for adaptive optics systems,” *J. Opt. Soc. Am. A* **36**, 731–740 (May 2019).
- [30] Haffert, S. Y., Males, J. R., Close, L. M., Van Gorkom, K., Long, J. D., Hedglen, A. D., Guyon, O., Schatz, L., Kautz, M., Lumbres, J., et al., “Data-driven subspace predictive control of adaptive optics for high-contrast imaging,” *Journal of Astronomical Telescopes, Instruments, and Systems* **7**(2), 029001–029001 (2021).
- [31] Landman, R., Haffert, S. Y., Radhakrishnan, V. M., and Keller, C. U., “Self-optimizing adaptive optics control with reinforcement learning for high-contrast imaging,” *Journal of Astronomical Telescopes, Instruments, and Systems* **7**(3), 039002–039002 (2021).
- [32] Nousiainen, J., Rajani, C., Kasper, M., Helin, T., Haffert, S., Vérinaud, C., Males, J., Van Gorkom, K., Close, L., Long, J., et al., “Toward on-sky adaptive optics control using reinforcement learning-model-based policy optimization for adaptive optics,” *Astronomy & Astrophysics* **664**, A71 (2022).
- [33] Vigan, A., Dohlen, K., N’Diaye, M., Cantalloube, F., Girard, J. H., Milli, J., Sauvage, J.-F., Wahhaj, Z., Zins, G., Beuzit, J.-L., Caillat, A., Costille, A., Le Merrer, J., Mouillet, D., and Tourenq, S., “Calibration of quasi-static aberrations in exoplanet direct-imaging instruments with a zernike phase-mask sensor - iv. temporal stability of non-common path aberrations in vlt/sphere,” *A&A* **660**, A140 (2022).
- [34] Ragazzoni, R., Diolaiti, E., and Vernet, E., “A pyramid wavefront sensor with no dynamic modulation,” *Optics communications* **208**(1-3), 51–60 (2002).
- [35] Pourcelot, R., N’Diaye, M., Por, E. H., Laginja, I., Carbillet, M., Benard, H., Brady, G., Canas, L., Dohlen, K., Fowler, J., Lai, O., Maclay, M., McChesney, E., Noss, J., Perrin, M. D., Petrone, P., Pueyo, L., Redmond, S. F., Sahoo, A., Vigan, A., Will, S. D., and Soummer, R., “Low-order wavefront control using a Zernike sensor through Lyot coronagraphs for exoplanet imaging. Blind stabilization of an image dark hole,” *Astron. & Astrophys.* **663**, A49 (July 2022).
- [36] Pourcelot, R., Por, E. H., N’Diaye, M., Benard, H., Brady, G., Canas, L., Carbillet, M., Dohlen, K., Laginja, I., Lugten, J., Noss, J., Perrin, M. D., Petrone, P., Pueyo, L., Redmond, S. F., Sahoo, A., Vigan, A., Will, S. D., and Soummer, R., “Low-order wavefront control using a Zernike sensor through Lyot coronagraphs for exoplanet imaging. II. Concurrent operation with stroke minimization,” *Astron. & Astrophys.* **672**, A73 (Apr. 2023).
- [37] Zhu, X., Lin, D., Hao, Z., Wang, L., and He, J., “A VIPA Spectrograph with Ultra-high Resolution and Wavelength Calibration for Astronomical Applications,” *Astronomical Journal* **160**, 135 (Sept. 2020).

- [38] Carlotti, A., Bidot, A., Mouillet, D., Correia, J.-J., Jocou, L., Curaba, S., Delboulbé, A., Le Coarer, E., Rabou, P., Bourdarot, G., et al., “On-sky demonstration at palomar observatory of the near-ir, high-resolution viba spectrometer,” in [*Ground-based and Airborne Instrumentation for Astronomy IX*], **12184**, 523–543, SPIE (2022).